

Durham Research Online

Deposited in DRO:

06 May 2021

Version of attached file:

Accepted Version

Peer-review status of attached file:

Peer-reviewed

Citation for published item:

Lietard, Aude and Mensa-Bonsu, Golda and Verlet, Jan R. R. (2021) 'The effect of solvation on electron capture revealed using anion two-dimensional photoelectron spectroscopy.', *Nature chemistry.*, 13 (8). pp. 737-742.

Further information on publisher's website:

<https://doi.org/10.1038/s41557-021-00687-1>

Publisher's copyright statement:

Additional information:

Use policy

The full-text may be used and/or reproduced, and given to third parties in any format or medium, without prior permission or charge, for personal research or study, educational, or not-for-profit purposes provided that:

- a full bibliographic reference is made to the original source
- a [link](#) is made to the metadata record in DRO
- the full-text is not changed in any way

The full-text must not be sold in any format or medium without the formal permission of the copyright holders.

Please consult the [full DRO policy](#) for further details.

A new perspective on the effect of solvation on electron capture

Aude Lietard, Golda Mensa-Bonsu, Jan R. R. Verlet

Department of Chemistry, Durham University, Durham DH1 3LE, United Kingdom

Abstract

The reaction of low-energy electrons with neutral molecules to form anions plays an important role in chemistry, being involved in, for example, various biological and astrochemical processes. However, key aspects of electron–molecule interactions, such as the effect of incremental solvation on the initially excited electronic resonances, remain poorly understood. Here, 2D photoelectron spectroscopy of anionic anthracene and nitrogen-substituted derivatives — solvated by up to 5 water molecules — reveals that for an incoming electron, resonances red-shift with increasing hydration; but for the anion, the excitation energies to the resonances remain essentially the same. These complementary points of view show that the observed onset of enhanced anion formation for a specific cluster size is mediated by a bound excited state of the anion. Our findings suggest that polycyclic aromatic hydrocarbons may be more efficient at electron capture than previously predicted with important consequences for the ionisation fraction in dense molecular clouds.

Main text

Low-energy electrons are ubiquitous initiators of chemistry in diverse environments ranging from biological tissue^{1,2} to the interstellar medium.³ Despite this ubiquity, many aspects of the fundamental physical chemistry that underpins electron-driven chemistry (EDC) remain poorly understood. One particularly important aspect of EDC concerns the question of how solvent molecules affect electron capture, which is critical to establishing a link between gas-phase (isolated) and a condensed-phase EDC. Some computational work has been aimed at answering this question,^{4–8} but experiments that probe the evolution of gas-to-condensed phases are scarce and cannot probe mechanistic details.^{6,9–11} Here, a new method is used to uncover how incremental solvation can dramatically affect electron capture.

Electron capture in an electron-molecule reaction is enabled by excited states of the corresponding anion.^{12,13} Such resonances can temporarily hold on to an incoming electron. As the electron's kinetic energy is always positive, the total energy of the temporary anion will be above the neutral ground state. Hence, electron loss (autodetachment) is an open channel that typically proceeds very rapidly ($\ll 1$ ps). However, the nuclei can also move upon electron attachment and this can lead to internal conversion between resonances and ultimately to the ground state of the anion. It is the competition between nuclear dynamics and electron loss that determines the outcome of EDC.¹⁴ Experimentally, electron capture or dissociative electron attachment can be evidenced by mass-spectrometrically measuring anion yields that have recently shown that dissociative electron attachment can be impacted by solvation.^{6,9–11} More generally, locations and dynamics of resonances can be probed by electron transmission spectroscopy¹⁵ or electron energy loss spectroscopy (and its 2D variant)¹⁶. The extension of methods that probe the resonances directly to micro-solvated molecules is complicated because mass-selection is not possible for the neutral target.

Recently, we have developed anion 2D photoelectron spectroscopy as a complementary method to probe resonances.^{17,18} In this method, one starts from the anion and uses a photon to access the electron-molecule resonances. The photoelectron spectrum is then analogous to the electron energy loss spectrum and, by acquiring photoelectron spectra at many photon energies, a 2D map of the resonances and their dynamics can be constructed. A key benefit of the method is that the target can be mass-selected so that incremental introduction of solvent molecules can be studied in a controlled manner, which is critical if we wish to understand how solvation affects resonances.

Here, we probe the electron capture of anthracene ($C_{14}H_{10}$) and nitrogen-substituted anthracene molecules at low energies. Our specific interest in these molecules is from an astrochemical perspective. Polycyclic aromatic hydrocarbons (PAHs) are prevalent in the interstellar medium.^{19,20} In dense molecular clouds, PAHs are predicted to become the main negative charge carrier (instead of electrons).^{21–24} These dark ($A_V > 2$) and cold (10s K) dense clouds also contain dust and ice grains,²⁵ where solvent molecules condense onto small particles often made of silicates or PAHs.^{26–28} The most abundant solvent is H_2O ^{26,29} and heteroatoms are also commonly incorporated in PAHs.²⁰ From a bottom-up perspective, these molecular ice grains can be viewed as PAH-water clusters. By studying the electron capture dynamics of such clusters, we aim to gain insight into the impact H_2O molecules have on the electron capture efficiency of a small PAH. Anthracene is the smallest linear PAH with a positive electron affinity (EA)¹⁵ and therefore serves as an ideal system to probe such processes.³⁰ Here, we apply anion 2D photoelectron imaging to show that the electron capture efficiency increases dramatically when a specific number of water molecules are present, and we reveal a new framework in which the observations can be understood.

Results

Figure 1a shows the 2D photoelectron spectra for anthracene anions surrounded by water molecules, $\text{C}_{14}\text{H}_{10}^-(\text{H}_2\text{O})_n$ with $n = 0 - 5$. The 2D false colour maps present photoelectron counts as a function of the photoexcitation energy ($h\nu$) and outgoing electron kinetic energy (eKE). They are made up from a series of photoelectron spectra that have been normalised to their integrated signal to accentuate trends and to assist comparison between different clusters and species. Two main trends can be seen: diagonal features (eKE increases linearly with $h\nu$) and vertical features (eKE is approximately constant with $h\nu$). Diagonal features arise from the direct photodetachment of an electron to from ground or excited states of the neutral; vertical features arise from excitation to an electronic resonance of the anion, which then autodetaches. The photoexcited resonances in PAH^- are the same resonances populated in the corresponding electron-PAH reaction, where the energy of an incoming electron can be approximated as $h\nu - \text{EA}$.

The resonances in the first few eV of the continuum of $\text{C}_{14}\text{H}_{10}^-$ have been characterised previously³¹ and all the photoelectron features are in close agreement with the available results for electron spectroscopy on $\text{C}_{14}\text{H}_{10}$.^{15,32–34} Briefly, the diagonal feature at highest eKE corresponds to direct detachment leaving $\text{C}_{14}\text{H}_{10}$ in its ground state, S_0 . Extrapolating this feature to $\text{eKE} = 0$ eV yields the EA of $\text{C}_{14}\text{H}_{10}$ (0.53 eV), in agreement with previous work.³⁵ A second diagonal feature starting at $h\nu = 2.5$ eV corresponds to direct detachment leaving $\text{C}_{14}\text{H}_{10}$ in its first excited triplet state, T_1 .

The first vertical feature has an onset of $h\nu \sim 1.1$ eV and arises from photoexcitation to a $\text{C}_{14}\text{H}_{10}^-$ resonance, which autodetaches to form electrons with a constant kinetic energy. We have previously shown³¹ that at least 2 resonances contribute to the first vertical feature,

where a second resonance at $h\nu \sim 1.6$ eV undergoes an internal conversion to the lower resonance at 1.1 eV, from which the electron then autodetaches. At higher $h\nu$, other resonances can be excited.

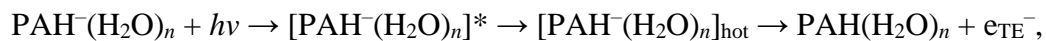
Figure 1a also shows the 2D photoelectron spectra of $\text{C}_{14}\text{H}_{10}^-(\text{H}_2\text{O})_n$ with $n = 1$ to 5. Diagonal features that correspond to direct detachment can be seen but these shift toward lower eKE as the number of water molecules increases. Hence, larger clusters have a larger EA, which arises predominantly from the cohesion energy of the water molecule to the $\text{C}_{14}\text{H}_{10}^-$ (mainly dipole-charge interaction). The measured EA for $\text{C}_{14}\text{H}_{10}^-(\text{H}_2\text{O})_1$ is in agreement with previous work.³⁶

The increase in EA as a function of n is shown in Figure 2a for $\text{C}_{14}\text{H}_{10}^-(\text{H}_2\text{O})_n$, where the ΔE represents the energy relative to S_0 . The cohesion energy for the first water molecule is approximately 240 meV and decreases with n . The energy of T_1 is also included in Figure 1a and shows that the singlet-triplet gap remains constant.

The hydrated clusters in Figure 1a also show vertical features. The onset of resonances is determined by the intersection of the autodetachment (vertical) feature with its corresponding direct detachment (diagonal) feature. These onsets are roughly at the same $h\nu$ for different n , suggesting that the resonances are approximately at the same excitation energy relative to the anion ground state. From the perspective of an electron approaching $\text{C}_{14}\text{H}_{10}(\text{H}_2\text{O})_n$, the resonances will thus appear at lower energy, as shown in Figure 2a. At $n = 2$, the EA of the cluster is almost degenerate with the excitation energy of the lowest resonance ($h\nu \sim 1.1$ eV). Hence, for $n > 2$, this resonance becomes a *bound* excited state of the anion.

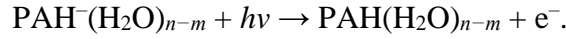
For $n \geq 2$, a significant change is observed in the 2D photoelectron spectra at the very low eKE. Specifically, over the first eV above the EA, a signal peaking at eKE = 0 eV is seen

that has an exponentially decaying spectral profile. An example of such a spectrum is shown in Figure 3a for $\text{C}_{14}\text{H}_{10}^-(\text{H}_2\text{O})_3$ at $h\nu = 2.20$ eV and compared to the spectrum of $\text{C}_{14}\text{H}_{10}^-$ at the same photon energy, which shows only a very small signal $\text{eKE} = 0$ eV. These very low energy signals are commonly seen in anion photoelectron spectroscopy and are a signature of statistical emission of electrons from a hot anionic ground state (thermionic emission).^{37–39} The apparition of thermionic emission evidences that the ground electronic state of the anion is reformed:



where $[\text{PAH}^-(\text{H}_2\text{O})_n]^*$ is the initial electron attachment resonance, $[\text{PAH}^-(\text{H}_2\text{O})_n]_{\text{hot}}$ is the anion electronic ground state, which has retained a total energy equal to $h\nu$ that has been redistributed amongst the internal degrees of freedom, and e_{TE}^- is the electron emitted by thermionic emission.

Additional verification that the ground state is recovered can be gained from the appearance of signal at eKE beyond the maximum allowed EA of the cluster. Specifically, signal is seen to extend to an eKE that correlates with the EA of the isolated $\text{C}_{14}\text{H}_{10}$ (shown as dashed diagonal lines in Figure 1a). An example of such a signal is shown in Figure 3b for $\text{C}_{14}\text{H}_{10}^-(\text{H}_2\text{O})_3$ excited at $h\nu = 1.15$ eV. This signal comes about because unimolecular decay of $[\text{PAH}^-(\text{H}_2\text{O})_n]_{\text{hot}}$ can also proceed by dissociation, $[\text{PAH}^-(\text{H}_2\text{O})_n]_{\text{hot}} \rightarrow \text{PAH}^-(\text{H}_2\text{O})_{n-m} + (\text{H}_2\text{O})_m$. The light field used in the experiments has a duration of ~ 5 ns and if dissociation occurs on a similar timescale, then a second photon can be absorbed by the daughter anion:



When $n = m$, the photoelectron signal arising from this second photodetachment process will correspond to the photoelectron spectrum of $\text{C}_{14}\text{H}_{10}^-$, as shown in Figure 3**b**.

We have also studied two nitrogen-substituted PAH (PANH) anions, acridine ($\text{C}_{13}\text{H}_9\text{N}^-$) and phenazine ($\text{C}_{12}\text{H}_8\text{N}_2^-$), and their hydrated clusters, $\text{C}_{13}\text{H}_9\text{N}^-(\text{H}_2\text{O})_n$ and $\text{C}_{12}\text{H}_8\text{N}_2^-(\text{H}_2\text{O})_n$, with $n = 1 - 5$. Their 2D photoelectron spectra are shown in Figure 1**b** and **c**, respectively. Comparing $\text{C}_{13}\text{H}_9\text{N}^-$ and $\text{C}_{12}\text{H}_8\text{N}_2^-$ to $\text{C}_{14}\text{H}_{10}^-$ reveals qualitatively similar trends of direct and indirect detachment channels in the first few eV of the continuum. The diagonal feature shows that the inclusion of the N atom increases the EA to 0.89 eV⁴⁰ and 1.22 eV⁴¹ for $\text{C}_{13}\text{H}_9\text{N}$ and $\text{C}_{12}\text{H}_8\text{N}_2$, respectively (c.f. 0.53 eV for $\text{C}_{14}\text{H}_{10}$). The first observable vertical features are shifted towards slightly higher $h\nu$. The emission profile of the vertical features, and therefore autodetachment dynamics, appear broadly similar for all species. The energies of all the electronic states derived from Figures 1**b** and **c** are shown in Figures 2**b** and **c**.

The adsorption of water molecules onto the PANH anions leads to similar trends as seen for $\text{C}_{14}\text{H}_{10}^-(\text{H}_2\text{O})_n$. The EA increases with increasing n as shown in Figure 2**b** and **c** while the excitation energy to the resonances remains essentially constant. Thermionic emission is apparent for $\text{PANH}^-(\text{H}_2\text{O})_n$ and has an onset for $\text{C}_{13}\text{H}_9\text{N}^-(\text{H}_2\text{O})_n$ at $n \geq 2$ and for $\text{C}_{12}\text{H}_8\text{N}_2^-(\text{H}_2\text{O})_n$ at $n \geq 1$. Also apparent from Figure 1 is that the range over which the ground state is recovered increases with number of N atoms.

Discussion

Electron scattering calculations have suggested that solvation has a significant effect on electron capture resonances.^{4–8} Fundamentally, our data do not disagree with this. From Figure 2, resonances appear at lower energies as the extent of solvation increases. However, from the perspective of the anion, a different view emerges, as illustrated in Figure 4. The energy gaps between the observed anion (doublet) states remains essentially constant with n . Hence, from the perspective of the anion, the energetics of the resonances do not change and the anion's electronic structure appears to be insensitive to solvation. The same is also observed for the PANHs in Figures 2b and c, even though the interaction with H₂O has changed for these anions as C₁₃H₉N has a dipole and both C₁₃H₉N and C₁₃H₈N₂ have lone-pair orbitals that contribute to the electronic structure.

While the differing perspectives of the same process (Figure 4) offer much insight, it is important to note that there are caveats that prevent a direct correlation of anion photoelectron spectroscopy as a probe for electron-molecule reactions. Specifically, the initial geometries are different in both cases.¹⁷ For the bare anion this difference is relatively small,³¹ but in the presence of H₂O molecules, there will be differences as the H₂O reorient to stabilise the charge in the anion. Nevertheless, upon electron attachment to a resonance and the formation of a temporary negative ion, H₂O will reorient to stabilise the resonance. Hence, the EA will increase as consequence of the dynamics of H₂O and if complete reorganisation is possible, then the anion picture becomes valid. The librational motion of H₂O can be very fast ($\ll 100$ fs),⁴² especially in interstellar ices based on its observed frequency at ~ 1000 cm⁻¹,⁴³ suggesting that reorientation can be competitive with autodetachment.

Given the insensitivity of the electronic structure of the PAH anion to solvation, why should the electron capture probability change so abruptly at a specific n ? The energetics summarised in Figure 2 and 4 offer a clear explanation. As the lowest resonance decreases in energy with increasing n (from the perspective of an electron-molecule reaction), it becomes a bound state at some n because the EA is increasing. For $\text{C}_{14}\text{H}_{10}^-(\text{H}_2\text{O})_n$, this occurs when $n > 2$ and appears to be directly correlated with the large enhancement of thermionic emission (ground state formation of the anion). The same argument holds for the studied PANHs. For $\text{C}_{13}\text{H}_8\text{N}_2^-(\text{H}_2\text{O})_n$, the number of water molecules required to render the electron resonance a bound excited state is smaller as shown in Figure 2c, because the electron affinity of $\text{C}_{13}\text{H}_8\text{N}_2$ is larger.

A bound excited state of the anion can facilitate electron capture in two ways. First, vibrational levels of the bound state remain above threshold (vibrational resonances) and these could accept the low-energy incoming electron. Rapid intramolecular vibrational redistribution can then inhibit autodetachment so that internal conversion to the ground electronic state can become the dominant decay path. Second, in the case of the PAHs studied here, a low energy electron can populate the higher-lying resonance (D_2 in Figure 2). For $\text{C}_{14}\text{H}_{10}^-$, we have shown that this resonance internally converts to the D_1 resonance.³¹ From the D_1 resonance, the electron is lost but, when D_1 becomes bound at $n > 2$, this autodetachment channel is closed and internal conversion to the ground state will dominate. This is shown schematically in Figure 4. The bound electronic state of the anion acts as an intermediate to form the ground electronic state of $\text{C}_{14}\text{H}_{10}^-(\text{H}_2\text{O})_{n>2}$. Large enhancements of electron capture mediated by bound electronic states has previously been observed for a quinone derivative.⁴⁴

Figure 1 shows that the resonances are not limited to a very narrow energy range. In dense molecular clouds, electrons thermalise to their surrounding temperature of a few 10s K

so that the electron energies are very low and in general < 100 meV.³ Figure 1 clearly shows that there are a range of energies, including the very low electron energies, over which electron capture will be efficient. This is particularly the case for the N-substituted PAH clusters, which show efficient thermionic emission over a very wide range of electron impact energies.

The above conclusions could affect the fractional abundance of PAH^- in dense molecular clouds. Models predict that PAHs become the dominant carrier of negative charge with $n_C > 30$, where the number of carbon atoms in the PAHs, n_C , is a determining factor to predict the electron attachment rate.^{21–24} Our results show that the availability of a bound state of the anion is also likely to be an important factor, as well as any micro-environment. Such factors are not presently included in models. Moreover, the dominant depletion mechanism for PAH^- in these models is photodetachment. Figure 1 shows that this process is in fact inhibited in the presence of solvent molecules because the resonance population can reform the ground state of the anion. The combined effects of additional PAH^- formation pathways together with a reduced destruction rate will lead to a higher abundance of PAH^- . From an astronomical perspective, the enhanced ability of PAHs to mop up and hold onto a negative charge shifts the overall ionisation fraction in dense molecular clouds, which is a determining factor in star formation.^{45,46} Specifically, the ionisation fraction will be decreased because PAHs are much more efficient at neutralising cations than electrons are. The exothermicity of neutralisation reactions is: (1) offset by the positive electron affinity of the PAH; and (2) redistributed amongst the internal degrees of freedom of the PAH, making it less likely to dissociate a cation.⁴⁷ With regards to both these points, the addition of solvent molecules increases both EA and the ability to absorb excess energy, not only because there are more degrees of freedom but also because the cluster can evaporate the solvent molecules as shown in Figure 3b. Given that the average energy of electrons in a molecular cloud is

< 100 meV, evaporation of a single water molecule will remove ~ 200 meV, which is sufficient to form a stable anion.

In conclusion, we have shown that anion 2D photoelectron spectroscopy offers new opportunities to probe electron-driven chemistry in complex environments. Electron attachment can be dramatically enhanced by the presence of water molecules because of the formation of an anion bound state as the resonances decrease in energy with increased solvation. While resonance energies change from the viewpoint of an electron-molecule reaction, they do not from the anion's perspective. We speculate that this concept could be quite general and may apply to many other electron-molecule reactions, especially those involving π^* resonances. This is supported by our finding that the electronic structure of the anions studied here is insensitive to solvation despite the chemical substitutions introduced. Our findings may also apply to other solvents. Water is generally a strongly interaction solvent, especially with anions, but this does not appear to have impacted the anion's electronic structure. Hence, the increased electron capture probability in the presence of H₂O may also be a feature for other molecules present in typical ice grains (e.g. CO, CO₂, NH₃, MeOH). The anions formed are open-shell (radical) species and are thus reactive and likely to be important sources of reactivity with all elements present to form prebiotic molecules.

References (main text)

1. Alizadeh, E. & Sanche, L. Precursors of Solvated Electrons in Radiobiological Physics and Chemistry. *Chem. Rev.* **112**, 5578–5602 (2012).
2. Boudaïffa, B., Cloutier, P., Hunting, D., Huels, M. A. & Sanche, L. Resonant Formation of DNA Strand Breaks by Low-Energy (3 to 20 eV) Electrons. *Science* **287**, 1658–1660 (2000).

3. Ingólfsson, O. *Low-Energy Electrons: Fundamentals and Applications*. (CRC Press, 2019).
4. Fabrikant, I. I., Caprasecca, S., Gallup, G. A. & Gorfinkiel, J. D. Electron attachment to molecules in a cluster environment. *J. Chem. Phys.* **136**, 184301 (2012).
5. Smyth, M., Kohanoff, J. & Fabrikant, I. I. Electron-induced hydrogen loss in uracil in a water cluster environment. *J. Chem. Phys.* **140**, 184313 (2014).
6. Kočíšek, J., Pysanenko, A., Fárník, M. & Fedor, J. Microhydration Prevents Fragmentation of Uracil and Thymine by Low-Energy Electrons. *J. Phys. Chem. Lett.* **7**, 3401–3405 (2016).
7. Sieradzka, A. & Gorfinkiel, J. D. Theoretical study of resonance formation in microhydrated molecules. I. Pyridine-(H₂O)_n, n = 1,2,3,5. *J. Chem. Phys.* **147**, 034302 (2017).
8. McAllister, M. *et al.* Solvation Effects on Dissociative Electron Attachment to Thymine. *J. Phys. Chem. B* **123**, 1537–1544 (2019).
9. Lengyel, J. *et al.* Electron-triggered chemistry in HNO₃/H₂O complexes. *Phys. Chem. Chem. Phys.* **19**, 11753–11758 (2017).
10. Poštulka, J., Slavíček, P., Fedor, J., Fárník, M. & Kočíšek, J. Energy Transfer in Microhydrated Uracil, 5-Fluorouracil, and 5-Bromouracil. *J. Phys. Chem. B* **121**, 8965–8974 (2017).
11. Meißner, R. *et al.* Low-energy electrons transform the nimorazole molecule into a radiosensitiser. *Nat. Commun.* **10**, 2388 (2019).
12. Schulz, G. J. Resonances in Electron Impact on Diatomic Molecules. *Rev. Mod. Phys.* **45**, 423–486 (1973).
13. Christophorou, L. G. *Electron–Molecule Interactions and their Applications*. (Academic Press, 1984).

14. Horke, D. A., Li, Q., Blancafort, L. & Verlet, J. R. R. Ultrafast above-threshold dynamics of the radical anion of a prototypical quinone electron-acceptor. *Nat. Chem.* **5**, 711–717 (2013).
15. Jordan, K. D. & Burrow, P. D. Temporary anion states of polyatomic hydrocarbons. *Chem. Rev.* **87**, 557–588 (1987).
16. Regeta, K. & Allan, M. Autodetachment Dynamics of Acrylonitrile Anion Revealed by Two-Dimensional Electron Impact Spectra. *Phys. Rev. Lett.* **110**, 203201 (2013).
17. Anstöter, C. S., Bull, J. N. & Verlet, J. R. R. Ultrafast dynamics of temporary anions probed through the prism of photodetachment. *Int. Rev. Phys. Chem.* **35**, 509–538 (2016).
18. Anstöter, C. S. *et al.* Mode-Specific Vibrational Autodetachment Following Excitation of Electronic Resonances by Electrons and Photons. *Phys. Rev. Lett.* **124**, 203401 (2020).
19. Tielens, A. g. g. m. Interstellar Polycyclic Aromatic Hydrocarbon Molecules. *Annu. Rev. Astron. Astrophys.* **46**, 289–337 (2008).
20. Tielens, A. G. G. M. The molecular universe. *Rev. Mod. Phys.* **85**, 1021–1081 (2013).
21. Omont, A. Physics and chemistry of interstellar polycyclic aromatic molecules. *Astron. Astrophys.* **164**, 159–178 (1986).
22. Lepp, S. & Dalgarno, A. Polycyclic aromatic hydrocarbons in interstellar chemistry. *Astrophys. J.* **324**, 553–556 (1988).
23. Allamandola, L. J., Tielens, A. G. G. M. & Barker, J. R. Interstellar polycyclic aromatic hydrocarbons - The infrared emission bands, the excitation/emission mechanism, and the astrophysical implications. *Astrophys. J. Suppl. Ser.* **71**, 733–775 (1989).
24. Wakelam, V. & Herbst, E. Polycyclic Aromatic Hydrocarbons in Dense Cloud Chemistry. *Astrophys. J.* **680**, 371–383 (2008).

25. Draine, B. T. Physics of the Interstellar and Intergalactic Medium. *Phys. Interstellar Intergalactic Medium Bruce T Draine Princet. Univ. Press 2011 ISBN 978-0-691-12214-4* (2011).
26. Allamandola, L. J., Bernstein, M. P., Sandford, S. A. & Walker, R. L. Evolution of Interstellar Ices. *Space Sci. Rev.* **90**, 219–232 (1999).
27. Geers, V. C. *et al.* Lack of PAH emission toward low-mass embedded young stellar objects. *Astron. Astrophys.* **495**, 837–846 (2009).
28. Bergin, E. A. & Tafalla, M. Cold Dark Clouds: The Initial Conditions for Star Formation. *Annu. Rev. Astron. Astrophys.* **45**, 339–396 (2007).
29. Boogert, A. C. A. *et al.* The c2dSpitzerSpectroscopic Survey of Ices around Low-Mass Young Stellar Objects. I. H₂O and the 5–8 μ m Bands^{1,2}. *Astrophys. J.* **678**, 985–1004 (2008).
30. Garcia-Sanz, A., Carelli, F., Sebastianelli, F., Gianturco, F. A. & Garcia, G. Dynamics of formation of anthracene anions in molecular clouds and protoplanetary atmospheres. *New J. Phys.* **15**, 013018 (2013).
31. Mensa-Bonsu, G., Lietard, A., Tozer, D. J. & Verlet, J. R. R. Low energy electron impact resonances of anthracene probed by 2D photoelectron imaging of its radical anion. *J. Chem. Phys.* **152**, 174303 (2020).
32. Burrow, P. D., Michejda, J. A. & Jordan, K. D. Electron transmission study of the temporary negative ion states of selected benzenoid and conjugated aromatic hydrocarbons. *J. Chem. Phys.* **86**, 9–24 (1987).
33. Gallup, G. A. Stable negative ions and shape resonances in a series of organic molecules. *J. Chem. Phys.* **139**, 104308 (2013).

34. Carelli, F., Gianturco, F. A., Satta, M. & Sebastianelli, F. Attaching electrons to a 3-ring acene: Structures and dynamics of anions in gas-phase anthracene. *Int. J. Mass Spectrom.* **365–366**, 377–383 (2014).
35. Kregel, S. J., Thurston, G. K. & Garand, E. Photoelectron spectroscopy of anthracene and fluoranthene radical anions. *J. Chem. Phys.* **148**, 234306 (2018).
36. Schiedt, J. & Weinkauff, R. Photodetachment photoelectron spectroscopy of mass selected anions: anthracene and the anthracene-H₂O cluster. *Chem. Phys. Lett.* **266**, 201–205 (1997).
37. Campbell, E. E. B. & Levine, R. D. Delayed Ionization and Fragmentation en Route to Thermionic Emission: Statistics and Dynamics. *Annu. Rev. Phys. Chem.* **51**, 65–98 (2000).
38. Andersen, J. U., Bonderup, E. & Hansen, K. Thermionic emission from clusters. *J. Phys. B At. Mol. Opt. Phys.* **35**, R1 (2002).
39. Adams, C. L., Hansen, K. & Weber, J. M. Vibrational Autodetachment from Anionic Nitroalkane Chains: From Molecular Signatures to Thermionic Emission. *J. Phys. Chem. A* **123**, 8562–8570 (2019).
40. Kokubo, S., Ando, N., Koyasu, K., Mitsui, M. & Nakajima, A. Negative ion photoelectron spectroscopy of acridine molecular anion and its monohydrate. *J. Chem. Phys.* **121**, 11112–11117 (2004).
41. Castro, K. P. *et al.* Incremental Tuning Up of Fluorous Phenazine Acceptors. *Chem. – Eur. J.* **22**, 3930–3936 (2016).
42. Bakker, H. J., Rezus, Y. L. A. & Timmer, R. L. A. Molecular Reorientation of Liquid Water Studied with Femtosecond Midinfrared Spectroscopy. *J. Phys. Chem. A* **112**, 11523–11534 (2008).

43. Maldoni, M. M., Egan, M. P., Robinson, G., Smith, R. G. & Wright, C. M. The phase of H₂O ice and the librational band in OH231.8+4.2: new interpretations. *Mon. Not. R. Astron. Soc.* **349**, 665–677 (2004).
44. Bull, J. N., West, C. W. & Verlet, J. R. R. On the formation of anions: frequency-, angle-, and time-resolved photoelectron imaging of the menadione radical anion. *Chem. Sci.* **6**, 1578–1589 (2015).
45. Nielbock, M. *et al.* The Earliest Phases of Star formation (EPoS) observed with Herschel: the dust temperature and density distributions of B68. *Astron. Astrophys.* **547**, A11 (2012).
46. Rosu-Finsen, A., Lasne, J., Cassidy, A., McCoustra, M. R. S. & Field, D. Enabling star formation via spontaneous molecular dipole orientation in icy solids. *Astrophys. J.* **832**, 1 (2016).
47. Bates, D. R. & Herbst, E. Dissociative Recombination: Polyatomic Positive Ion Reactions with Electrons and Negative Ions. in *Rate Coefficients in Astrochemistry* (eds. Millar, T. J. & Williams, D. A.) 41–48 (Springer Netherlands, 1988). doi:10.1007/978-94-009-3007-0_3.

Acknowledgements

We thank Martin McCoustra for useful discussions. This work has been funded by the EPSRC (EP/R023085/1 and EP/M507854/1).

Author Contributions

J.R.R.V. conceived the project. A.L. and G. M.-B. performed the experiments. A.L. analysed the data. All discussed the results and J.R.R.V. and A.L. wrote the paper.

Competing Interests Statements

The authors declare no competing interests.

Figure Captions

Figure 1: 2D photoelectron spectra of PA(N)H water cluster anions. Photoelectron spectra of **a** anthracene ($C_{14}H_{10}$), **b** acridine ($C_{13}H_9N$) and **c** phenazine ($C_{12}H_8N_2$) anions and their clusters with n water molecules. Photoelectron spectra have been recorded with $h\nu$ increments of 50 meV for **a** and 100 meV increment for **b** and **c**. Each photoelectron spectrum has been normalised to its total signal intensity. Figure 1 is constructed from a total of 754 photoelectron images. Dashed lines represent the expected electron kinetic energy for photoelectrons ejected to form the ground and first (triplet) excited states of the neutral if no water molecules were present. Resonances can be identified by deviations from diagonal photoelectron signal trends. For the three molecules, the position of the resonances with increasing n remain essentially the same. For $(C_{14}H_{10})^-_{n \geq 2}$, $(C_{13}H_9N)^-_{n \geq 2}$, and $(C_{12}H_8N_2)^-_{n \geq 1}$, a new and intense photoelectron feature appears at very low kinetic energy (thermionic emission) that highlights the regeneration of the anionic ground state from the excited resonances.

Figure 2: Energies of electronic states of PA(N)H water cluster anions. Energies are derived from Figure 1 and are presented relative to S_0 for **a** $C_{14}H_{10}^-$, **b** $C_{13}H_9N^-$ and **c** $C_{12}H_8N_2^-$ as a function of the cluster size, n . Circles represent neutral states (S_0 and T_1) formed upon direct photodetachment; squares represent the ground and excited states of the

anion (respectively D_0 and D_1 , D_2 , D_i , D_j), where D_1 is the lowest-lying resonance. The uncertainty in the position of the resonances is on the order of ± 0.1 eV. Lines are guides for the eyes and the grey shaded area represents the lowest electron detachment continuum. As n increases, the energy of the resonances decreases with respect to S_0 . However, the energy gaps between the resonances and the D_0 state remains approximately equal (i.e. they are parallel). When the energy of D_1 energy becomes lower than that of S_0 , the D_1 resonance becomes a bound state of the anion and can facilitate electron capture.

Figure 3: Photoelectron spectra of $C_{14}H_{10}^-$ and $C_{14}H_{10}^-(H_2O)_3$. Photoelectron spectra recorded at **a** $h\nu = 2.20$ eV and **b** 1.15 eV. The appearance of thermionic emission is seen in **a** for $C_{14}H_{10}^-(H_2O)_3$. Photodetachment from $C_{14}H_{10}^-$ by a second photon is highlighted in **b** following the initial photodetachment from $C_{14}H_{10}^-(H_2O)_3$. Both thermionic emission and fragmentation evidence the formation of the anionic ground state following excitation indicating that the resonances accessed at these photon energies are efficient at electron capture.

Figure 4: Schematic of electron capture process by a PAH in the presence of water molecules. Electron capture process is shown from the perspective of the anion following photoexcitation (left) and the neutral following electron excitation (right). The anion ground state (blue solid line), the neutral ground state (black dotted line) and the anion resonances (red solid line) energetics are shown as a function of solvation. Vertical downward arrows (yellow) indicate electron emission and wiggly arrows (green) show internal conversion. From the anion's viewpoint, the excitation energies remain the same, but from the neutral's perspective, electron-molecule resonances decrease in energy. These complementary views

demonstrate how electron-molecule resonances decrease with solvation, ultimately leading to a bound state that mediates electron capture.

Methods

Anionic water clusters of anthracene ($C_{13}H_{10}$), acridine ($C_{13}H_9N$) and phenazine ($C_{12}H_8N_2$) were produced in a molecular beam source.⁴⁸ The solid samples were heated to ~480 K in a heated pulsed valve and its vapour pressure was seeded in Ar at a pressure of 3 bar with H_2O present by adding a drop of water to the carrier gas line. The mixture was expanded into vacuum and crossed by an electron beam (300 eV), forming anions (as well as cations and neutrals). The vibrational temperature of the ions is likely to be on the order of a few 10s K as they are effectively cooled in the supersonic expansion and water molecules condense onto the PAH. Anions were extracted from the expansion using a perpendicular time-of-flight mass-spectrometer. At the focus of the mass-spectrometer, a specific m/z anion packet was irradiated with light from a nanosecond Nd:YAG pumped OPO. Emitted photoelectrons were projected onto a position sensitive detector using a velocity map imaging spectrometer.⁴⁹ The resolution was on the order of 3% ($\Delta eKE/eKE$) and all spectra were calibrated using iodide. Photoelectron images were reconstructed to offer the corresponding spectra using polar onion peeling.⁵⁰

References (for methods)

48. Rogers, J. P., Anstöter, C. S., Bull, J. N., Curchod, B. F. E. & Verlet, J. R. R. Photoelectron Spectroscopy of the Hexafluorobenzene Cluster Anions: $(\text{C}_6\text{F}_6)_n^-$ ($n = 1 - 5$) and $\text{I}-(\text{C}_6\text{F}_6)$. *J. Phys. Chem. A* **123**, 1602 (2019).
49. Eppink, A. T. J. B. & Parker, D. H. Velocity map imaging of ions and electrons using electrostatic lenses: Application in photoelectron and photofragment ion imaging of molecular oxygen. *Rev. Sci. Instrum.* **68**, 3477–3484 (1997).
50. Roberts, G. M., Nixon, J. L., Lecointre, J., Wrede, E. & Verlet, J. R. R. Toward real-time charged-particle image reconstruction using polar onion-peeling. *Rev. Sci. Instrum.* **80**, 053104 (2009).

Data Availability

The raw photoelectron images that are used to construct Figure 1, together with their photoelectron spectra, are available at doi:10.5281/zenodo.4314369. All other results are derived from these data.

Code Availability

Photoelectron images have been analysed using polar onion peeling, which is available at <https://www.github.com/adinatan/PolarOnionPeeling> (Matlab version) or <http://www.verlet.net/research.html> (Labview version).